DOI: 10.1534/genetics.105.048934

A Novel Murine Gene, *Sickle tail*, Linked to the *Danforth's short tail* Locus, Is Required for Normal Development of the Intervertebral Disc

Kei Semba,*,† Kimi Araki,* Zhengzhe Li,* Ken-ichirou Matsumoto,*,† Misao Suzuki,‡ Naoki Nakagata,§ Katsumasa Takagi,† Motohiro Takeya, Kumiko Yoshinobu,†† Masatake Araki,†† Kenji Imai,‡‡ Kuniya Abe§§ and Ken-ichi Yamamura*,[1]**

**Division of Developmental Genetics, Institute of Molecular Embryology and Genetics, Kumamoto University, Kumamoto 862-0976, Japan, †Department of Orthopaedic Surgery, Kumamoto University School of Medicine, Kumamoto 860-8556, Japan, ‡Division of Transgenic Technology, Institute of Resource Development and Analysis, Kumamoto University, Kumamoto 860-0811, Japan, §Division of Reproductive Engineering, Institute of Resource Development and Analysis, Kumamoto University, Kumamoto 860-0811, Japan, **Department of Cell Pathology, Kumamoto University School of Medicine, Kumamoto 860-8556, Japan, ††Division of Bioinformatics, Institute of Resource Development and Analysis, Kumamoto University, Kumamoto 860-0811, Japan, ‡‡Institute of Developmental Genetics, GSF-National Research Center for Environment and Health, 85764 Neuherberg, Germany and §§Technology Development Team for Mammalian Cellular Dynamics, BioResource Center, RIKEN, Tsukuba, Ibaraki 305-0074 Japan*

Manuscript received July 29, 2005
Accepted for publication September 26, 2005

ABSTRACT

We established the mutant mouse line, B6;CB-*Skt*^{GtAyu8021IMEG} (*Skt*^{Gt}), through gene-trap mutagenesis in embryonic stem cells. The novel gene identified, called *Sickle tail* (*Skt*), is composed of 19 exons and encodes a protein of 1352 amino acids. Expression of a reporter gene was detected in the notochord during embryogenesis and in the nucleus pulposus of mice. Compression of some of the nuclei pulposi in the intervertebral discs (IVDs) appeared at embryonic day (E) 17.5, resulting in a kinky-tail phenotype showing defects in the nucleus pulposus and annulus fibrosus of IVDs in *Skt*$^{Gt/Gt}$ mice. These phenotypes were different from those in *Danforth's short tail* (*Sd*) mice in which the nucleus pulposus was totally absent and replaced by peripheral fibers similar to those seen in the annulus fibrosus in all IVDs. The *Skt* gene maps to the proximal part of mouse chromosome 2, near the *Sd* locus. The genetic distance between them was 0.95 cM. The number of vertebrae in both [*Sd* +/+ *Skt*^{Gt}] and [*Sd Skt*^{Gt}/+ +] compound heterozygotes was less than that of *Sd* heterozygotes. Furthermore, the enhancer trap locus *Etl4*^{lacZ}, which was previously reported to be an allele of *Sd*, was located in the third intron of the *Skt* gene.

THE notochord is an integral component of the axial structure of vertebrates, functions as a signaling center during embryogenesis, and plays essential roles in patterning of both somites and the neural tube (Ang and Rossant 1994; Wilson *et al.*1995; Chiang *et al.*1996). In addition, the notochord has major roles in vertebral column formation. In the mouse, the notochord is a continuous rod of constant diameter extending from the hypophysis to almost the tip of the tail at embryonic day (E) 9.5. At E10.5–E11.5, signals from the notochord induce the migration, proliferation, and fusion of the sclerotome to form a continuous and unsegmented perichordal tube around the notochord and neural tube. At 12.5, mesenchyme acquires a characteristic metameric pattern of densely packed areas caudally and loosely packed areas cranially. Some densely packed cells move cranially and give rise to the annulus fibrosus of the future intervertebral disc (IVD). The remaining densely packed cells fuse with the immediately caudal loosely packed cells to form the cartilaginous primordia of the vertebral bodies. Notochord cells located in the vertebral body of cranial regions start to relocate into intervertebral regions (Paavola *et al.* 1980; Rufai *et al.* 1995; Aszodi *et al.* 1998). At E13.5, the vertebral regions are enlarged and chondrified. The notochord proliferates and undergoes hypertrophy to form the gelatinous center of the intervertebral disc, called the nucleus pulposus. This nucleus is surrounded by the circularly arranged fibers of the annulus fibrosus. These two structures together constitute the IVD (Langman 1969; Theiler 1988). At E14.5, nearly all chondrocytes are hypertrophied. Starting from E14.5, the annulus fibrosus can be subdivided into a fibrous outer annulus and a cartilaginous inner annulus. At E16.0, notochord cells complete relocation from vertebral regions into

Sequence data from this article have been deposited with the EMBL/GenBank Data Libraries under accession nos. AB125594, AB125595, and AB033043.

[1]*Corresponding author:* Division of Developmental Genetics, Institute of Molecular Embryology and Genetics, Kumamoto University, 4-24-1 Kuhonji, Kumamoto 862-0976, Japan.
E-mail: yamamura@gpo.kumamoto-u.ac.jp

intervertebral regions. Failures in somite, neural tube, and notochord formation are closely correlated with vertebral malformations. However, the mechanisms that underlie the formation of IVDs are largely unknown.

In the mouse, several mutations are known to affect the formation of the vertebral column due to functional defects in the notochord, including *Danforth's short tail* (*Sd*) and the enhancer trap line (*Etl4*^{lacZ}). *Sd*, located on chromosome 2 (Lane and Birkenmeiser 1993; Alfred *et al.* 1997), is a semidominant mutation affecting the development of the vertebral column and the urogenital system (Dunn *et al.* 1940; Gruneberg 1953, 1958). At E9.5, the notochord shows discontinuities. At E11.5, mesenchymal organization around the notochord is abnormal. At E13.5, the notochord is fragmented and does not show proliferation and dilatation. Chondrification is much reduced in vertebral regions. Thus, an early reduction of the notochord results in cellular degeneration in the sclerotome, leading to reduced vertebral bodies and a characteristic short tail due to a reduced number of caudal vertebrae. Homozygous *Sd* animals show a similar but much more severe tailless phenotype. In the enhancer trap line, *Etl4*^{lacZ}, a reporter (*lacZ*) gene was inserted near the *Sd* locus and was expressed in the notochord, mesonephric mesenchyme, and apical ectoderm ridge (Gossler *et al.* 1989; Korn *et al.* 1992; Maatman *et al.* 1997; Zachgo *et al.* 1998). *Etl4*^{lacZ} homozygotes exhibited kinks in the caudal region of their tails and a synergistic genetic interaction between *Etl4*^{lacZ} and *Sd* was observed. Genetically, *Etl4*^{lacZ} and *Sd* are separated by 0.75 cM. Interestingly, attenuation or enhancement of the *Sd* phenotype was observed when the *Etl4*^{lacZ} insertion was in a *cis*- or *trans*-conformation, respectively. This suggests that *Etl4*^{lacZ} is an allele of *Sd*, presumably by trapping a *cis*-regulatory element of the *Sd* gene, and that *Sd* is a gain-of-function mutation (Zachgo *et al.* 1998). Nevertheless, neither the *cis*-element nor the trapped gene has been identified.

In this study, we report a new mutant mouse line, *Skt*^{Gt}, obtained by gene-trap mutagenesis in embryonic stem (ES) cells. *Skt*$^{Gt/Gt}$ mice exhibit a kinky tail in the caudal vertebral columns due to malformation of the IVDs. The gene identified, *Sickle tail* (*Skt*), was expressed in the notochord, its derivative nucleus pulposus, and in the mesonephros. Interestingly, the *Skt* gene maps to the proximal part of mouse chromosome 2, near the locus for *Sd*, and the *lacZ* insertion site in *Etl4*^{lacZ} was found to be located in the third intron of the *Skt* gene. Furthermore, a cumulative effect of the *Skt*^{Gt} mutation on the *Sd* mutant was observed.

MATERIALS AND METHODS

Generation and genotyping of mutant mice: The gene-trap method using the pU-8 trap vector was previously described (Araki *et al.* 1999). Chimeric mice were produced by the aggregation method using ES gene-trap clones and morulas of ICR (Charles River, Wilmington, MA) mice, and the chimeric mice were mated with C57BL/6 (CLEA) females to obtain F_1 heterozygotes. *Sd* mice were purchased from the Jackson Laboratory (Bar Harbor, ME) and propagated by *in vitro* fertilization. *Sd*+/+ *Skt*^{Gt} mice were generated by mating *Sd*+/+ + mice (C57BL/6 genetic background) to *Skt*$^{Gt/Gt}$ mice with a C57BL/6 genetic background. One heterozygote carrying the *Sd* mutation and the *Skt*^{Gt} insertion on the same chromosome (*Sd Skt*^{Gt}/+ +; *cis*-configuration) was obtained through mating between *trans*-heterozygotes and wild-type C57BL/6 mice. *Sd* mice were distinguished by external inspection. Genotyping for *Skt*^{Gt} alleles was done with PCR using tail genomic DNA as a template. For the wild-type allele, the 5′ primer, GTS (5′-CCACCCCTACATGTGTCTTT-3′), and the 3′ primer, GTA (5′-CGAGTAAGTAACATCCCTCC-3′) located in the 14th intron, were used to generate a 339-bp wild-type fragment. To detect the trapped allele, the 5′ primer, called Z1 (5′-GCGTT ACCCAACTTAATCG-3′), and the Z2 (5′-TGTGAGCGAGTAA CAACCCG-3′) located in *lacZ* gene, were used to generate a 320-bp fragment.

Skeletal preparations: After tail skins were peeled off, tails were fixed in 95% ethanol for 3 days. Tails were cleared by placing in 1% KOH for 1 day and were stained in alizarin red for 1 day until the bone was red. Excess stain was removed with 2% KOH. After removing excessive alizarin red stain, tails were transferred to glycerol (Hogan *et al.* 1994).

To count the number of vertebral bodies, we examined all mice by X-ray photography. We counted the number of normal vertebral bodies, that is, those without obvious malformations, but did not consider the size reduction observed in the vertebral bodies of *Sd* mutants.

Cloning of genomic DNA and cDNA: Plasmid rescue to obtain flanking genomic DNA was performed as described (Araki *et al.* 1999). The 5′-end of the cDNA of the trapped gene was isolated by 5′-rapid amplification of cDNA ends (5′-RACE) using the 5′-RACE system (Invitrogen, Carlsbad, CA). Total RNA from a B6;CB-*Skt*^{GtAyu8021IMEG} gene-trapped ES clone was extracted by using Sepasol-RNA I (NACALAI TESQUE, Kyoto, Japan), and then poly(A)+ RNA was isolated with an oligo(dT) column (Takara Biomedicals, Shiga, Japan). First-strand cDNA synthesis from 1 μg of poly(A)+ RNA was performed with reverse transcriptase from ReverScript (Wako, Osaka, Japan) and with the primer SA13 (5′-TCTGAAACT CAGCCTTGAGC-3′) in the splice acceptor (SA) sequence. After dCTP tailing with terminal deoxynucleotidyl transferase (Invitrogen), cDNA was purified using a QIAquick nucleotide removal kit (QIAGEN, Chatsworth, CA). The initial PCR was performed using the primer SA10 (5′-AGCAGTGAAGGCTGT GCGA-3′) in the SA sequence and the anchor primer (5′-GGCCACGCGTCGACTAGTACGGGiiGGGiiGGGiiG-3′) (Invitrogen). Then, nested PCR was performed using primer 63 (5′-GCTTGTCCTCTTTGTTAGGG-3′) in the SA sequence and the amplification primer (5′-GGCCACGCGTCGACTAGTAC-3′) in the anchor primer sequence. Amplified fragments were then sequenced directly by the dideoxy-chain termination method using Big Dye terminator cycle sequencing (Perkin-Elmer, Foster City, CA).

RT–PCR analysis: RT–PCR was performed using the Thermoscript RT–PCR system (Invitrogen) according to the manufacturer's instructions. The PCR was performed using the primers a–f in the sense and antisense sequences in the *Skt* gene. The sequences of the primers used are as follows: primer-a, 5′-TCACCATGAAGATGCTGGAG-3′; primer-b, 5′-CTACAG TAAGCACTCGCTGAC-3′; primer-c, 5′-ACTCCTCAGCCTTG ATGAAC-3′; primer-d, 5′-GTGGTGGTAAGTCCTGATCC-3′; primer-e, 5′-GCCACCTTAAAGACACTAGG-3′; and primer-f, 5′-TGAGGAGGAAGAGGTAGTAG-3′. The PCR conditions were

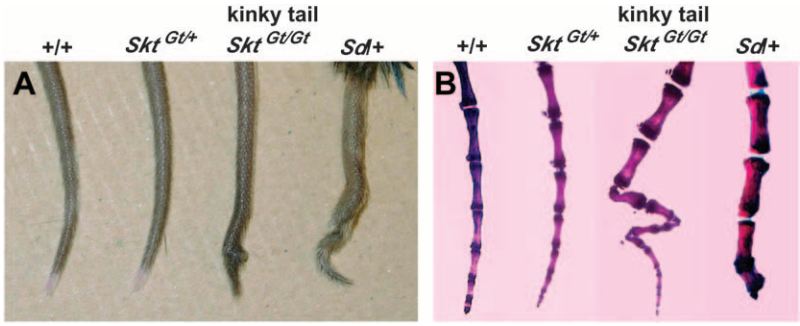

FIGURE 1.—(A) Tail phenotype of 8-week-old mice. $Skt^{Gt/Gt}$ mice had kinked tails compared to wild-type, $Skt^{Gt/+}$, and heterozygous *Sd* mice. (B) Alizarin red whole-mount preparations of the tails of 8-week-old mice. $Skt^{Gt/Gt}$ mice confirmed this kinky-tail phenotype. *Sd* mice showed decreased numbers of vertebrae with truncation at the caudal vertebrae.

94° for 1 min, 55° for 2 min, and 72° for 2 min using 0.5 units of Taq polymerase for 30 cycles.

Northern blot analysis: Total RNA and poly(A)+ mRNA isolated from ES cells and embryo and adult tissues were electrophoresed on a 0.7% denaturing formaldehyde-MOPS-containing agarose gel and transferred to a positively charged nylon membrane (Roche). After baking at 80° for 1 hr, the membrane was prehybridized and then hybridized using the *Skt* gene-specific RNA probes and the *lacZ* RNA probes prepared using DIG RNA labeling and detection kit (Roche).

Detection of β-galactosidase (*lacZ*) activities: Whole-mount X-gal staining was performed according to the method of ALLEN *et al.* (1988). Samples were fixed for 30 min at room temperature in fix solution [1% formaldehyde, 0.2% glutaraldehyde, and 0.02% NP-40 in phosphate-buffered saline (PBS)]. Fixed samples were washed two times in PBS and incubated overnight at 30° in staining solution (5 mM potassium ferricyanide, 5 mM potassium ferrocyanide, 2 mM $MgCl_2$, 0.5% X-gal in PBS). Samples were rinsed twice in PBS, postfixed in 4% paraformaldehyde, and made transparent using benzylalcohol/benzylbenzoate (1:2) after dehydration with a series of ethanol steps (25, 50, 70, 100, and 100%, 1 hr each). Adult tissues were fixed in 4% paraformaldehyde in PBS. Tissue sections of 10 μm were prepared and stained overnight at 30° with X-gal in staining solution. After staining, sections were counterstained with Fast Red. For the section of the intervertebral discs, after X-gal stained tails were refixed in 3.7% formaldehyde/PBS, the caudal vertebral bones were demineralized in Plank–Rychlo solution and embedded in paraffin according to standard procedures. Sections of 8 μm were prepared and counterstained with Nuclear Fast red.

Construction and transfection of the *Skt* expression vector: To clone the full open reading frame (ORF) of the *Skt* gene, RT–PCR was performed using the Thermoscript RT–PCR system. The initial PCR was performed using the primer ORFS1 in the sense strand upstream from the start codon in the *Skt* gene (5′-ACCGGAGTGGAGACTAGTTG-3′) and primer ORFA1 in the antisense strand downstream from the stop codon in the *Skt* gene (5′-TGCATGAGGCCTTGAACGATACAG-3′). Then, nested PCR was performed using the sense-strand primer ORFS2 (5′-TTTCTGCGAGCTTTCCGAAC-3′) and the antisense-strand primer ORFA2 (5′-ACCTTGGTCCTAATAGGATCTG GC-3′). The PCR conditions used were 94° for 1 min, 58° for 1 min, and 72° for 3 min using 1.0 unit of LA Taq polymerase (Takara Biomedicals) for 25 cycles. The 4.1-kb PCR products were cloned into the pGEM-T vector (Promega, Madison, WI). This cDNA ORF was confirmed by sequencing and cloned into the pCAGGS expression vector (NIWA *et al.* 1991). Transfection into BMT10 cells (GERARD and GLUZMAN 1985) was carried out by the lipofection method using LipofectAMINE reagent (Invitrogen).

Western blot analysis: BMT10 cells and 40 pieces of the nucleus pulposus of caudal IVDs of adult mice were homogenized in 2× sample buffer (100 mM Tris HCl pH 6.8, 4% SDS, 12% β-mercaptoethanol, 20% glycerol). Extracts were electrophoresed on a 6.0% polyacrylamide gel, transferred to a nitrocellulose filter (Immobilon, Millipore, Bedford, MA), and detected using anti-Skt antibodies with the ECL detection system (Amersham, Arlington Heights, IL).

Immunohistochemistry: Tails were fixed in 4% paraformaldehyde in PBS. The caudal vertebral bones were demineralized in 0.24 M EDTA·2Na, 0.22 M EDTA·4Na solution for 48 hr and embedded in paraffin blocks. Sections of the IVDs were immunostained with anti-Skt antibodies by the avidin–biotin complex method (Vector Laboratories, Burlingame, CA). Sections were counterstained with hematoxylin.

RESULTS

Generation of *Sickle tail* mutant mice: A gene-trap ES clone was isolated by the exchangeable gene-trap method using the trap vector pU-8 (ARAKI *et al.* 1999). We obtained eight chimeric mice of which three were germline chimeras. Heterozygous animals appeared normal and were fertile. About half (35/66) of the homozygotes, however, showed a peculiar kinky-tail phenotype (Figure 1A and Table 1). This mutant mouse line was designated as B6;CB-$Skt^{GtAyu8021IMEG}$, in which *Skt* means *Sickle tail* because of the characteristic shape of the tail. Shortened and curved caudal vertebrae were apparent by the age of 2 weeks and were restricted to the 20–25th caudal vertebrae (Figure 1B). In contrast, heterozygous *Sd* mice showed short tails with truncation of vertebral columns at the 6th caudal vertebral body on average (Figures 1B and 7A) as reported previously. In $Skt^{Gt/Gt}$ mice, no other skeletal abnormality was observed by bone X-ray examination (data not shown).

TABLE 1

Summary of genotyping of 4-week-old mice from Skt^{Gt} heterozygote matings

		Gt/Gt	
+/+	*Gt*/+	Kinked	Normal[a]
60	151	35 (53%)	31

[a] All normal-looking homozygotes showed deformity of the caudal discs by histological analysis.

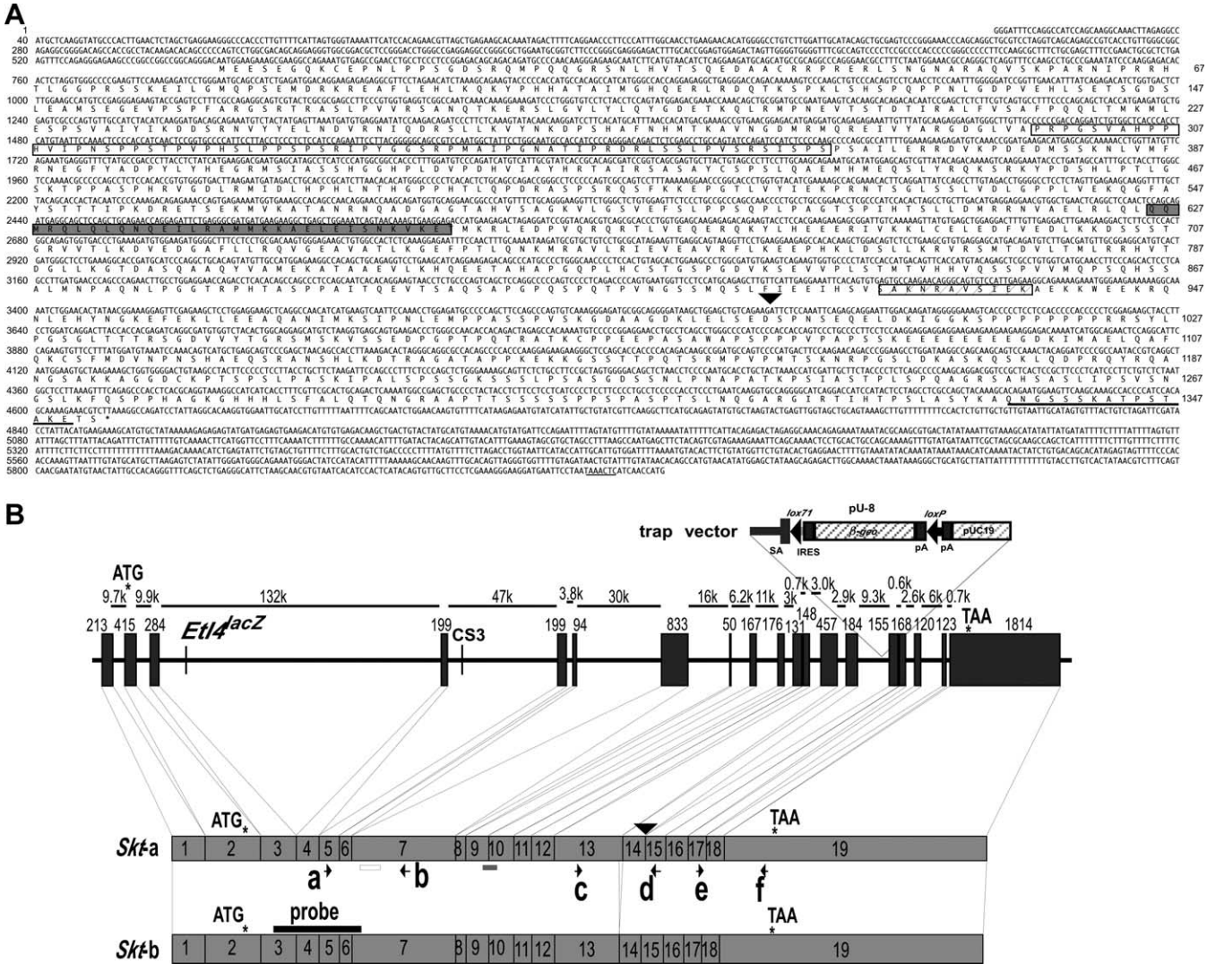

FIGURE 2.—Identification of the trapped gene *Skt*. (A) The nucleotide sequence of the *Skt* cDNA and predicted amino acid sequence. The open box indicates the pro-rich region at the N terminus and the shaded box indicates the coiled-coil region in the middle. The striped box indicates the sequence deleted in *Skt*-b by alternative splicing. The 15-amino-acid peptide used for the production of anti-Skt antibodies is shown by underlining. The polyadenylation signal is underlined at the 3′-end of the nucleotide sequence. The nucleotide sequence is numbered on the left side and the amino acid sequence is numbered on the right side. (B) Genomic structure of the *Skt* gene. (Top) Exon-intron structure of the *Sickle tail* gene. The trap vector, pU-8, was inserted into the 14th intron. Sizes of exons and introns are given. (Bottom) Two transcripts produced from the *Skt* allele. There are at least two types of *Skt* transcripts: one contains all the exons (termed *Skt*-a) and the other lacks 33 bp of the 13th exon (termed *Skt*-b). Arrows (a–f) indicate the location of the primers used for RT–PCR analyses in Figure 3, A–C, to detect the expression of each part of the *Skt* transcripts. The solid bar represents a probe used for Northern blotting. The open and shaded boxes indicate the pro-rich region and the coiled-coil region, respectively. The start and stop codons of the *Skt* gene are shown by asterisks. A sequence with high homology to the CS3 in node/notochord enhancers is located in the fourth intron of the *Skt* gene 106 kb downstream of the insertion site of *Etl4*^{lacZ}.

Characterization of the integration site of the trap vector: To characterize the gene-trap locus, we cloned and sequenced genomic DNA fragments flanking the gene-trap vector. A single copy of the vector was integrated into the genome as determined by Southern blot analysis using genomic DNA samples extracted from *Skt*^{Gt} mice. Three base pairs of genomic DNA were deleted at the integration site of the trap vector. Using PCR amplification on genomic DNA samples, the genotype of offspring from the heterozygous intercross was easily determined (data not shown).

Identification of the *Sickle tail* gene: To identify the gene trapped, we performed 5′-and 3′-RACE. The sequence of the ORF of the trapped gene was determined by compiling sequences of 5′- and 3′-RACE products and of EST that showed 100% homology to the RACE products. We thus obtained a cDNA sequence comprising 5930 nucleotides (accession no. AB125594) that encodes a putative protein of 1352 amino acids with a predicted molecular weight of 147 kDa (Figure 2A). This gene was termed *Skt*. The protein contains a proline-rich region (amino acid residues 298–364) and a coiled-coil region

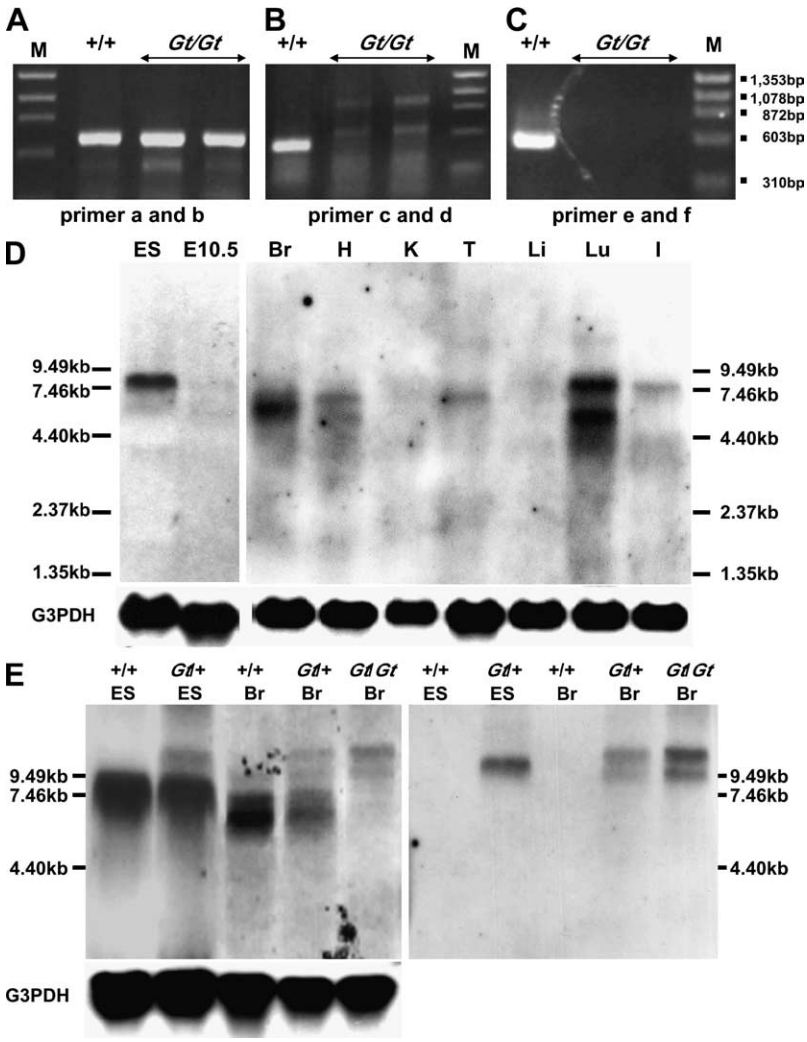

FIGURE 3.—Analyses of *Skt* transcripts. (A–C) RT–PCR analyses using E10.5 embryos to detect *Skt* transcripts in wild-type (+/+) and $Skt^{Gt/Gt}$ embryos. The transcripts containing nucleotide sequences upstream of the insertion site of the trap vector were detected in both wild-type and $Skt^{Gt/Gt}$ embryos (A). The transcripts containing nucleotide sequences downstream of the *Skt* sequence were not detected in $Skt^{Gt/Gt}$ embryos (B and C). M, molecular marker. (D) Northern blot analyses to detect *Skt* mRNA in the wild-type ES cells, E10.5 embryo, and 8-week-old mice, using the *Skt*-specific probe in the 5′-region (see Figure 2B). Total RNA (10 μg) from TT2 ES cells, wild-type E10.5 embryos, mRNA (5 μg) from wild-type organs, and a *Skt* RNA probe were used for Northern blotting. (E) Northern blot analyses to detect *Skt* and β-*geo* fusion transcripts. Total RNA (20 μg) from TT2 and heterozygous (*Gt*/+) ES cells, wild-type (+/+), heterozygous (*Gt*/+), and homozygous (*Gt/Gt*) adult brains was used for Northern blotting. The *Skt* RNA probe or *lacZ* RNA probe was used in the left and right panels, respectively. Br, brain; H, heart; K, kidney; T, testis; Li, liver; Lu, lung; I, intestine.

(amino acid residues 626–656) as determined by analysis using Lupas's algorithm (LUPAS *et al.* 1991). An ATG codon is located at nucleotide positions 559–561. This codon is most likely the initiation codon, because there is a Kozak sequence surrounding this ATG codon (KOZAK 1996): *i.e.*, there is a G residue following the ATG codon and an A residue three nucleotides upstream. A BLAST search of the amino acid sequence deduced from the *Skt* cDNA sequence revealed 80.6% homology with an uncharacterized human protein, KIAA 1217 (accession no. AB033043), and no other evolutionarily conserved protein was identified.

Sequence comparison of *Skt* cDNA with the murine genome sequence in the public Mouse Genome Resources (http://www.ncbi.nlm.nih.gov/genome/guide/mouse/) revealed that the *Skt* gene consists of 19 exons spanning >300 kb and that the ATG codon is located in the second exon (Figure 2B). The trap vector was integrated in the 14th intron, resulting in the disruption of the Skt protein at position 998 (arrowhead in Figure 2, A and B). Sequence analyses of fusion transcripts revealed the presence of two fusion transcripts with the β-*geo* sequence: *Skt-a*, containing the 1st–14th exons, and *Skt-b*, lacking 33 bp of the 13th exon from *Skt-a* (Figure 2B). In any case, a truncated protein lacking 355 amino acids encoded by exons 15–19 in the C-terminal region is expected to be produced from the Skt^{Gt} allele.

RT–PCR and Northern blot analyses: We performed RT–PCR using wild-type and $Skt^{Gt/Gt}$ embryos at E10.5. RT–PCR with primers a and b located within the 5′-region of the integration site and detected the expected band in both embryos (Figure 3A). Using RT–PCR with two primer pairs—c in the 5′-region and d in the 3′-region of the integration site and primers e and f within the 3′-region of the integration site—we could not detect any product in $Skt^{Gt/Gt}$ embryos (Figure 3, B and C), indicating the absence of *Skt* mRNA containing exons 15–19 in $Skt^{Gt/Gt}$ embryos.

To analyze the size and expression pattern of *Skt* mRNA, we performed Northern blot analysis using the *Skt*-specific probe in the 5′-region (see Figure 2B). As shown in Figure 3D, a major band of 8 kb and a minor band of 6.5 kb were detected in wild-type ES cells. In wild-type whole embryos at E10.5, the 8- and 6.5-kb bands were also detected, although the expression levels were low. Surprisingly, Northern blot analysis using mRNA

from wild-type adult organs revealed the presence of four different mRNA transcripts, 5.5, 6.5, 7.0, and 8.0 kb. The faint 7.0-kb and strong 6.5-kb bands in the brain, the 7.0- and 5.5-kb bands in the heart, the 7.0-kb band in the testis, the 8.0- and the 5.5-kb bands in the lung, and the 8.0-kb band in the intestine were detected (Figure 3D). We then examined the presence of the *Skt* and β-*geo* fusion mRNA (Figure 3E). In $Skt^{Gt/+}$ ES cells, an expected 10.5-kb band representing the fusion transcript containing β-*geo* was detected with both the *Skt* and *lacZ* probes, although the intensity was weaker than that of the 8-kb band of the endogenous transcript. In the $Skt^{Gt/+}$ and $Skt^{Gt/Gt}$ adult brains, two bands of 10.5 and 9.5 kb were detected with the *Skt* probe (Figure 3E, left), and these bands were also hybridized with the *lacZ* probe (Figure 3E, right), confirming that both transcripts corresponded to the fusion mRNA containing β-*geo*. This result indicates the existence of alternative splicing in the upstream region of the insertion site. Northern blot analysis using mRNA from wild-type adult heart revealed the presence of two different transcripts, the 7- and 5.5-kb bands when the *Skt* probe was used. However, in the Skt^{Gt} adult heart, one 9.5-kb band was detected with the *lacZ* probe (data not shown). This result indicates that alternative splicing in the heart may occur in the downstream region of the insertion site, leading to the production of the 7- and 5.5-kb bands. The largest size of mRNA is 8 kb, which is larger than that of the predicted cDNA sequence comprising 5930 nucleotides (accession no. AB125594). As described below, the anti-Skt antibodies recognized only an ~150-kDa protein corresponding to the predicted molecular weight of 147 kDa in extracts from the nucleus pulposus of the caudal IVDs (see lane 4 in Figure 6A). Thus, the 8-kb mRNA may contain untranslated regions at both the 5′- and 3′-ends and splicing may occur in each untranslated region. Further study will be required to determine the untranslated regions.

Formation of vertebral column and β-*geo* expression in Skt^{Gt} mice: We examined formation of the vertebral column in Skt^{Gt} mice during the embryonic, fetal, and postnatal periods (E8.0, E8.5, E9.0, E9.5, E10.5, E11.5, E12.5, E13.5, E14.5, 15.5, E16.5, E17.5, E18.5, E19.5, newborn, and 2 weeks of age) by histological analysis with and without X-gal staining. Before E8.0, the β-*geo* gene was expressed in the chorion, but not in the embryo (Figure 4A). At E8.5 (Figure 4B) and E9.0 (Figure 4C), intense staining was detected in the notochord. At E11.5, the notochord and the mesonephros expressed β-*geo* strongly (Figure 4, D–F). In addition, sections of E11.5 embryos showed β-*geo* expression in the epithalamus sulcus, roof of the neopallial cortex, lens vesicle, inner layer of retina, heart (atrium and ventricle), surface of hepatic primordium, infundiblum, surface ectoderm, hind gut, and mesenchyme of the limb bud (data not shown). No abnormality was found in both vertebral and intervertebral regions up to E16.5. In the $Skt^{Gt/Gt}$ embryo at E17.5, compression was observed in some IVDs (Figure 4, I and J) of the $Skt^{Gt/Gt}$ embryo, but not in the wild-type embryo (Figure 4, G and H). In the $Skt^{Gt/Gt}$ neonate, the X-gal-positive cells in the nucleus pulposus were shifted to the periphery and the alignment of the vertebral bodies was undulated (Figure 4, M and N). At this stage, sizes of IVDs are the same as those of wild-type mice. In 2-week-old $Skt^{Gt/Gt}$ mice, the X-gal-positive notochord cells were dislocated to the left or right side and the nuclei pulposi were smaller and eccentric, resulting in the disappearance of normal IVDs (Figure 4, Q and R). In the $Skt^{Gt/+}$ embryo and mice, the X-gal-positive cells were positioned in the center of the vertebrae at any stage (Figure 4, G, K, and O). Interestingly, the expression of the reporter gene was much lower in the upper IVDs than in the fifth to seventh caudal IVD, coinciding with a relationship between the phenotype of the $Skt^{Gt/Gt}$ and strong expression in the caudal region of the tail.

Histological analyses of IVDs of $Skt^{Gt/Gt}$ and *Sd* mutant adult mice: In $Skt^{Gt/Gt}$ adults, the β-*geo* gene was also expressed in many tissues such as the corpus callosum in the brain, uriniferous tubules in kidney, cardiac muscle, Sertoli's cells in testes, and basal cells and outer root sheaths of hair follicles in skin (data not shown).

In normal adult mice, the nucleus pulposus was located in the center of IVDs at all levels of the vertebral column (Figure 5, A, D, G, and J). However, the nucleus pulposus in the IVDs of the tail region of $Skt^{Gt/Gt}$ mice contained an aggregation of notochord-like cells with fewer vacuoles than normal and were dislocated to the periphery (Figure 5, H and K). The nucleus pulposus in the upper regions appeared normal (Figure 1, B and E). Although histochemical analyses of embryos and newborns in the *Sd* mutant were reported by Paavola *et al.* (1980) and Theiler (1988), the histochemical analyses of the IVDs in *Sd* mutant adult mice have not previously been performed in detail. Thus, we analyzed the IVDs of the whole spine in *Sd* +/+ + mutant mice. Surprisingly, the IVDs were totally occupied by peripheral fibers similar to those seen in the annulus fibrosus and no nucleus pulposus was found within the IVDs (Figure 5, C and F). The degeneration of the nucleus pulposus in the center of caudal IVDs was occasionally observed (Figure 5, I and L). Although tail kinks of $Skt^{Gt/Gt}$ mice were restricted to the 20–25th caudal vertebrae (Figure 1B), an irregular boundary with direct contact between the nucleus pulposus and annulus fibrosus (Figure 5, O and P) was observed in the 5–25th caudal IVDs of $Skt^{Gt/Gt}$ mice, compared to the sharp boundary and fixed space observed between the nucleus pulposus and the fibrous layers of the annulus fibrosus in normal mice (Figure 5, M and N). In addition to the abnormalities of the nucleus pulposus in IVDs, the annulus fibrosus development was also impaired in $Skt^{Gt/Gt}$ mice as demonstrated by the thin fibrous layers of annulus fibrosus and the failure of fibrous adhesion in the vertebral bodies (Figure 5, Q and R). We also examined whether similar abnormalities were

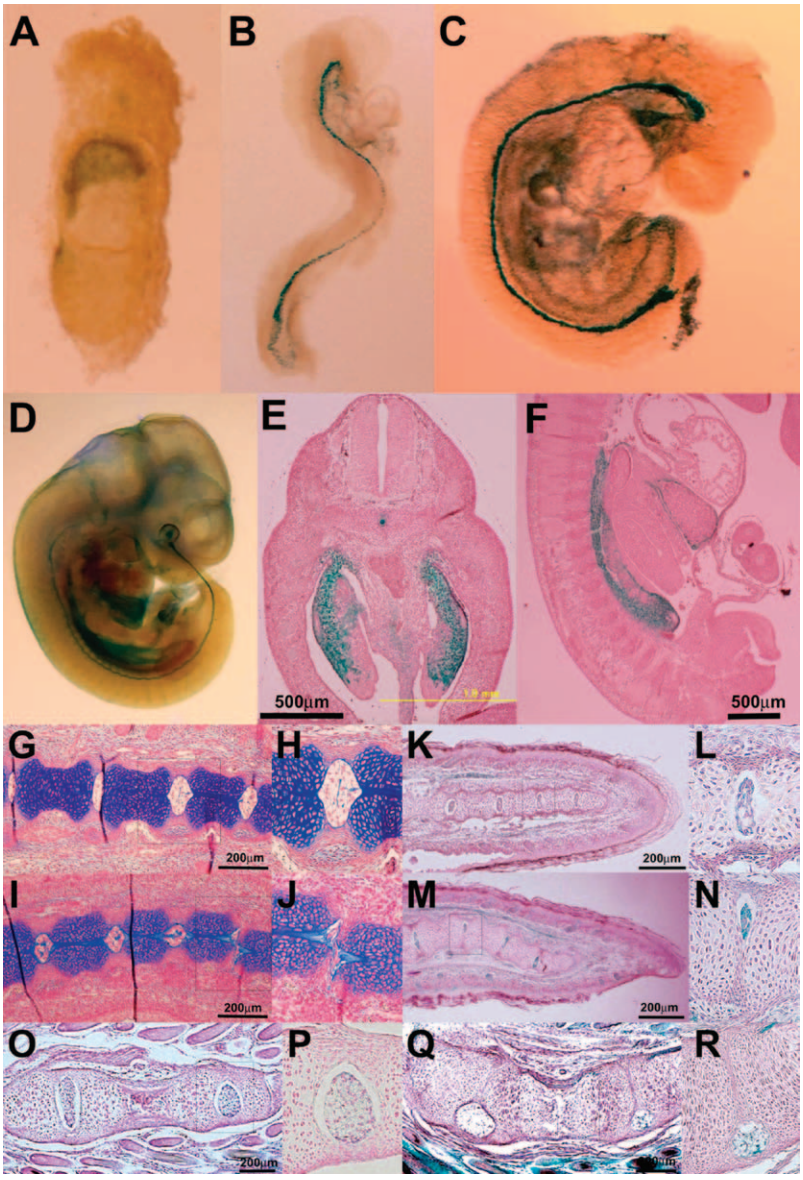

FIGURE 4.—β-*gal* expression and histological analyses in Skt^{Gt} mice. At E7.5 (A), the chorion was stained with X-gal, but the midline region of the embryo was not stained. At E8.5 (B) and E9.0 (C) intense staining was detected in the notochord. At E11.5 (D–F), the notochord and the mesonephros expressed β-*geo* strongly in whole-mount X-gal staining (D), the frontal section (E), and the sagittal section (F). Sagittal sections of the tail bud of $Skt^{Gt/+}$ (G and H) and $Skt^{Gt/Gt}$ (I and J) embryos at E17.5. At E17.5, some IVDs were compressed in the tail bud of $Skt^{Gt/Gt}$ (J). Sagittal sections of the tail tips of newborn $Skt^{Gt/+}$ (K and L) and $Skt^{Gt/Gt}$ (M and N) mice. In the $Skt^{Gt/Gt}$ neonate, the vertebral body alignment was undulated (M and N). Sagittal sections of the tail tips of 2-week-old $Skt^{Gt/+}$ (O and P) and $Skt^{Gt/Gt}$ (Q and R) mice. In the 2-week-old $Skt^{Gt/Gt}$ mice, the X-gal-positive nuclei pulposi were dislocated to the periphery (Q and R). (H, J, L, N, P, and R) Higher magnification of the area indicated by the boxes in G, I, K, M, O, and Q, respectively. Sections (G–J) were stained with alcian blue and sections of X-gal staining (E, F, and K–R) were counterstained with Nuclear Fast red. Bars, 200 μm.

observed in the regions that did not have kinks in $Skt^{Gt/Gt}$ mice (Table 1). Surprisingly, histological analysis of externally normal tails of $Skt^{Gt/Gt}$ mice revealed the presence of similar IVD abnormalities such as dislocation of the nucleus pulposus and thin fibrous layers of the annulus fibrosus (Figure 5S) as found in kinked tails (Figure 5, Q and R). This IVD phenotype was observed over 10 generations in the progeny backcrossed to C57BL/6. Thus, the primary phenotype of $Skt^{Gt/Gt}$ mice is the deformity of IVDs in the tail region. These histological pictures were clearly distinct from those of *Sd* mice.

Analysis of Skt protein using anti-Skt antibody: The anti-Skt antibodies recognized an ~150-kDa protein corresponding to the predicted molecular weight of 147 kDa in the lysates of BMT10 cells transiently expressing the *Skt* cDNA by the CAG promoter as well as in extracts from the nucleus pulposus of the caudal IVDs. No band was detected in extracts from untreated BMT10 cells and BMT10 cells transfected with mock expression vector (Figure 6A). This is consistent with the notion that ATG at positions 559–561 and TAA at positions 4615–4617 in the *Skt* cDNA are the start codon and termination codon, respectively. As expected, the amount of Skt protein was decreased in $Skt^{Gt/+}$ mice and was below the detectable level in $Skt^{Gt/Gt}$ mice (Figure 6A). After immunohistochemical staining, the nucleus pulposus cells from upper caudal vertebral discs were positively stained in wild-type mice (Figure 6B, a and c), but not in $Skt^{Gt/Gt}$ mice (Figure 6B, b and d). At higher magnification, the staining was observed mainly in the cytoplasm of the nucleus pulposus cells, indicating cytoplasmic localization of the Skt protein. Since we could not produce antibodies against the N terminus, the expression of the truncated protein was not confirmed in $Skt^{Gt/Gt}$ mice.

Relationship of *Skt* with $Etl4^{lacZ}$ or *Sd* loci: Both the expression pattern of the *Skt* gene and the phenotype of Skt^{Gt} mutant mice were quite similar to those of $Etl4^{lacZ}$ mutant mice (ZACHGO *et al.* 1998). Furthermore, by examining

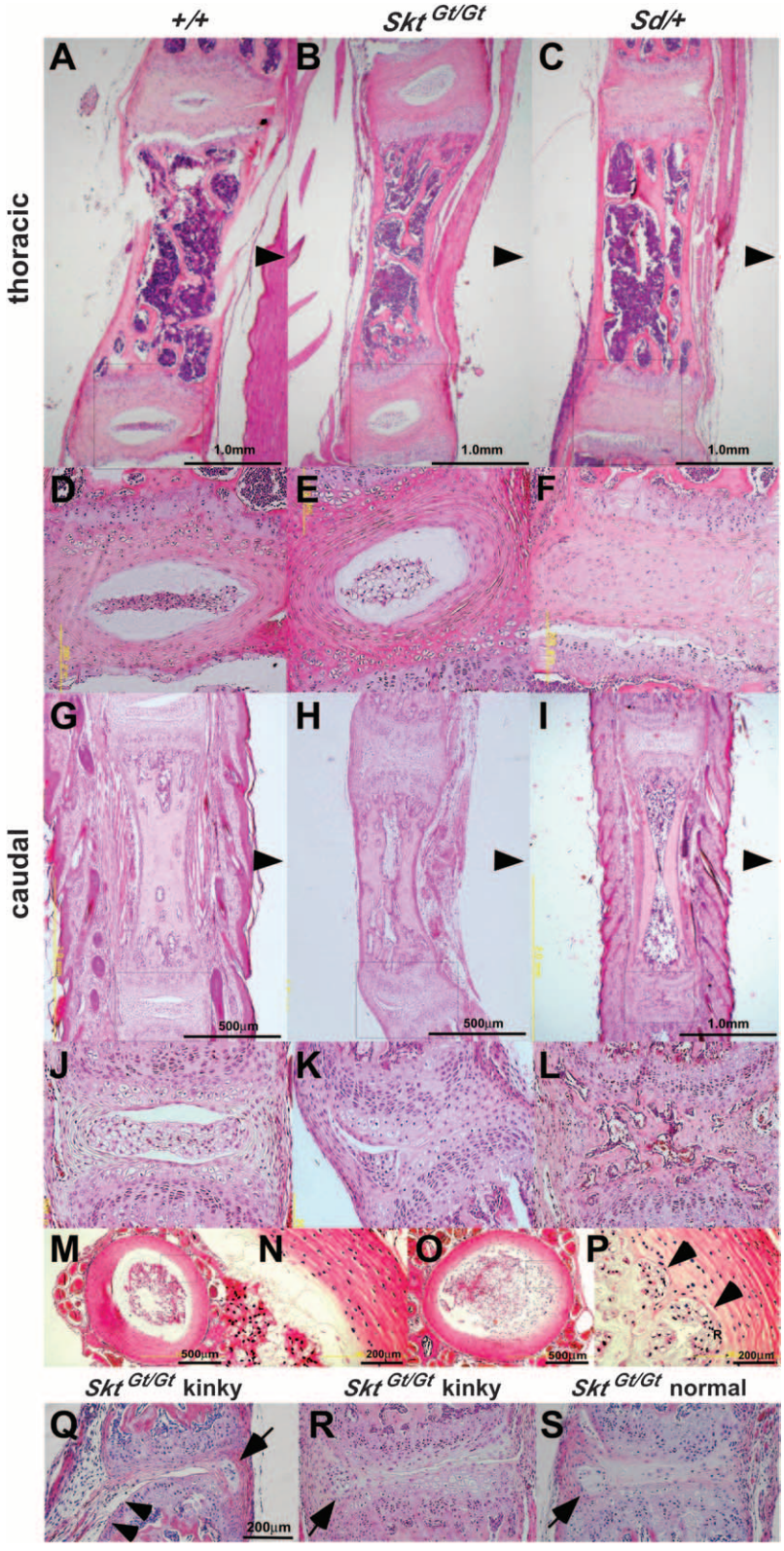

FIGURE 5.—Histological analyses of IVDs of $Skt^{Gt/Gt}$ and *Sd* mutant adult mice. Sagittal sections of the thoracic and caudal IVD from 8-week-old adult wild-type (A, D, G, and J), $Skt^{Gt/Gt}$ (B, E, H, and K), and heterozygous *Sd* mice (C, F, I, and L). (D, E, F, J, K, and L) Higher magnification of the area indicated by the boxes in A, B, C, G, H, and I, respectively. Arrowheads indicate the dorsal side. Axial sections of the upper caudal IVD in wild-type (M and N) and $Skt^{Gt/Gt}$ (O and P) 8-week-old mice. (N and P) Higher magnification of the area indicated by the boxes in M and O, respectively. The arrowheads in P indicate an irregular boundary with close contact between the nucleus pulposus and annulus fibrosus. (Q–S) The 20–25th caudal IVDs of $Skt^{Gt/Gt}$ 8-week-old mice. Impaired development of the annulus fibrosus in $Skt^{Gt/Gt}$ mice was demonstrated by the thin fibrous layers of annulus fibrosus (Q and R) and the failure of fibrous adhesion to the vertebral bodies (arrowhead in Q). Similar IVD abnormalities such as dislocation of the nucleus pulposus (arrow in Q–S) and impaired growth of the annulus fibrosus were observed in the non-kinked regions (S) and in the kinked regions (Q and S). Haematoxylin and eosin (HE) staining was used. Bars, 200 μm.

the reported primer sequences of the $Etl4^{lacZ}$ locus (MAATMAN *et al.* 1997), we found that the $Etl4^{lacZ}$ locus is located in the third intron of the *Skt* gene (Figure 2B) and that the distance between the integration sites of $Etl4^{lacZ}$ and Skt^{Gt} was 237 kb.

To examine the genetic distance and interaction between the Skt^{Gt} and *Sd* locus, we crossed Skt^{Gt} mice with *Sd* mice to produce the compound heterozygote (*Sd* +/+ Skt^{Gt}; *trans*-configuration). Then, these compound heterozygotes were used to analyze the recombination rate

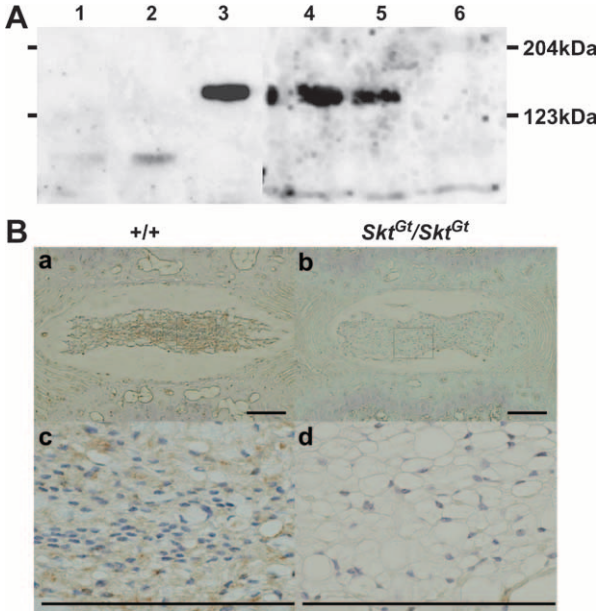

Figure 6.—Detection of the Skt protein. (A) Western blot analysis to detect Skt protein using extracts from untreated BMT10 cells (lane 1), BMT10 cells transfected with vector (lane 2), BMT10 cells transfected with the *Skt* expression vector (lane 3), and extracts of the nucleus pulposus of caudal IVDs from 8-week-old wild-type mice (lane 4), $Skt^{Gt/+}$ mice (lane 5), and $Skt^{Gt/Gt}$ mice (lane 6). An ~150-kDa protein corresponding to the predicted molecular weight of 147 kDa was detected in lanes 3, 4, and 5, but not in lane 6. The amount of Skt protein was reduced in the $Skt^{Gt/+}$ mutant (lane 5) and was below the detectable level in $Skt^{Gt/Gt}$ (lane 6). (B) Immunohistochemistry of frontal sections of the nucleus pulposus in upper caudal IVDs from adult 8-week-old mice using purified anti-Skt antibodies. Skt protein was detected in the cytoplasm of nucleus pulposus cells in wild-type (a and c), but not $Skt^{Gt/Gt}$, mice (b and d). (c and d) Higher magnification of the area indicated by the boxes in a and b, respectively. Bars, 200 μm.

between the two loci. As shown in Table 2, one compound heterozygote carrying the *Sd* mutation and the Skt^{Gt} insertion on the same chromosome (*Sd* Skt^{Gt}/+ +; *cis*-configuration) and two wild-type mice were obtained among 249 mice obtained by mating the *trans* compound heterozygote with the wild-type C57BL/6 mice, demonstrating that the *Sd* and Skt^{Gt} mutations were genetically separated. The genetic distance was calculated to be ~0.95 cM by combining the data from mating the [*Sd* Skt^{Gt}/+ +] (*cis*) compound heterozygote with the wild-type mice (Table 2).

To evaluate the effect of the Skt^{Gt} mutation on the tail phenotype in heterozygous *Sd* mice in either the *trans*- or the *cis*-configuration, the number of vertebrae was determined by X-ray analysis. Heterozygous *Sd* [*Sd* +/+ +] mice ($n = 22$) had a variable number of vertebrates and the vertebral columns were truncated at the sixth caudal vertebral body on average. Both *trans* [*Sd* +/+ Skt^{Gt}] ($n = 23$) and *cis* [*Sd* Skt^{Gt}/+ +] ($n = 10$) compound heterozygous mice had shorter tails, in which the vertebral columns were truncated at the second and third caudal vertebral body on average (Figure 7A). We examined whether the phenotype of [*Sd* Skt^{Gt}/+ Skt^{Gt}] neonatal mice is more severe than those of *trans* [*Sd* +/+ Skt^{Gt}] and *cis* [*Sd* Skt^{Gt}/+ +] compound heterozygous mice. Approximately 80% of [*Sd* Skt^{Gt}/+ Skt^{Gt}] neonatal mice died within 48 hr of birth and all mutant mice died within 2 weeks. In addition, as shown by making alcian blue/alizarin red whole-mount preparations of [*Sd* Skt^{Gt}/+ Skt^{Gt}] neonatal mice, [*Sd* Skt^{Gt}/+ Skt^{Gt}] neonatal mice had shorter tails than those of *trans* [*Sd* +/+ Skt^{Gt}] and *cis* [*Sd* Skt^{Gt}/+ +] compound heterozygous mice, in which the vertebral columns were truncated at the fourth sacral vertebral body on average, suggesting a cumulative effect of the Skt^{Gt} mutation on the *Sd* mutant.

To examine the pathologic effect of the *Skt* mutation on the *Sd* phenotype, we carried out histological analyses on the IVDs of *Sd* +/+ Skt^{Gt} and *Sd* Skt^{Gt}/+ + mutant mice. Both compound heterozygous mice showed IVD histology similar to that seen in *Sd* +/+ + mutant mice. The nucleus pulposus was totally absent and replaced by peripheral fibers similar to those seen in the annulus fibrosus in all IVDs (Figure 7B, a–h). These results suggest that the *Skt* mutation did not affect the histological picture of IVD in the *Sd* mutation. In addition, the expression pattern of the β-*geo* gene in the tail notochord was the same in both *trans* [*Sd* +/+ Skt^{Gt}] and *cis* [*Sd* Skt^{Gt}/+ +] compound heterozygous embryos at E9.5 and E13.5 (Figure 7C). The notochord of both *trans* and *cis* compound heterozygous embryos was thin and clearly stained at E9.5 (Figure 7C, a and d), and the X-gal-positive notochord was similarly fragmented in both *trans* and *cis* compound heterozygous embryos at E13.5 (Figure 7C, b, c, e, and f). This suggested that the *Sd* mutation did not affect *Skt* expression. In addition, this *trans*–*cis* test demonstrated that the double heterozygotes exhibited indistinguishable phenotypes in

TABLE 2

Distribution of the haplotypes among the 315 offspring of the backcross *Sd* +/+ Skt^{Gt} or *Sd* Skt^{Gt} /+ + × C57BL/6

Sd +/+ Skt^{Gt} × C57 BL/6				*Sd* Skt^{Gt}/+ + × C57 BL/6			
+ +/+ Skt^{Gt}	*Sd* +/+ +	*Sd* Skt^{Gt}/+ +	+ +/+ +	+ Skt^{Gt}/+ +	*Sd* +/+ +	*Sd* Skt^{Gt}/+ +	+ +/+ +
144	102	1	2	0	0	24	42

Sd, Skt^{Gt} compound heterozygotes were generated from crosses with an inbred laboratory strain (C57BL/6)

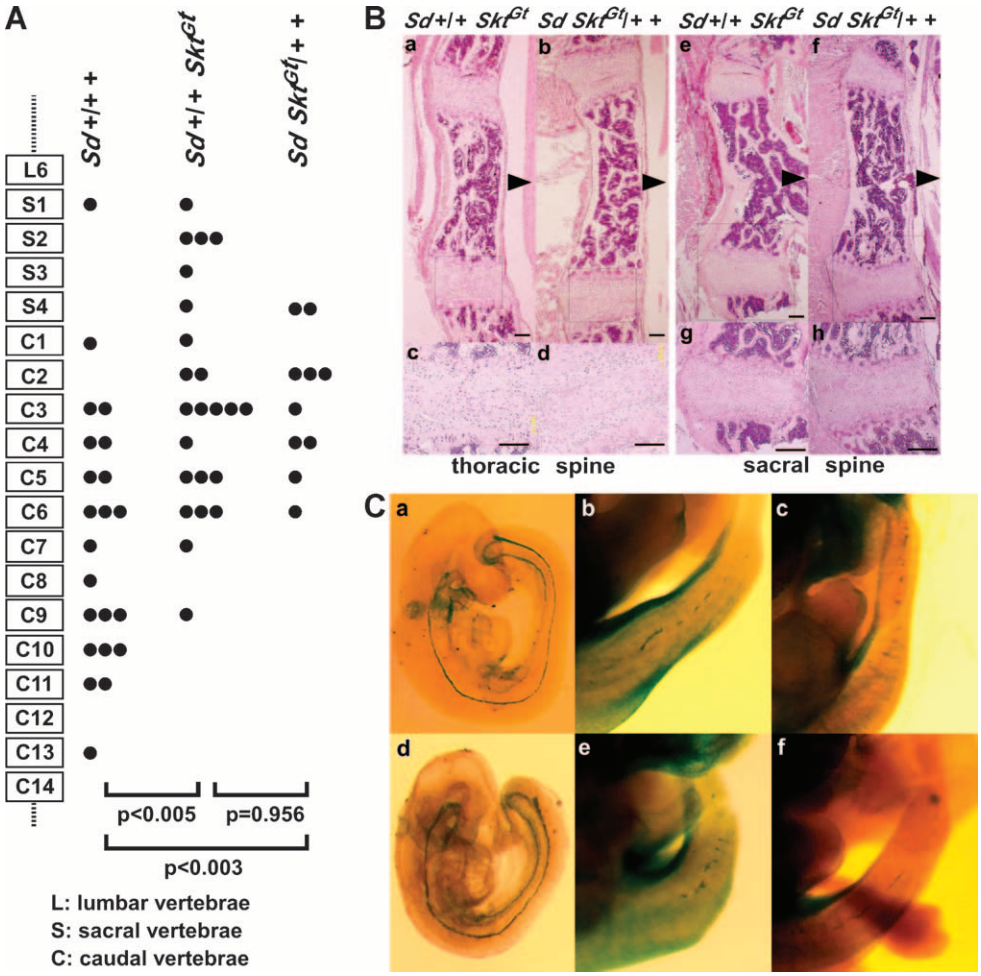

FIGURE 7.—(A) Schematic of axial levels and severity of vertebral malformations in compound mutant 8-week-old mice. A single solid circle indicates the level of the terminal vertebral body for a single mouse. In both *trans* and *cis* compound mutant mice, the degree of vertebral malformation is more severe than that in heterozygous *Sd* mice (*trans*, $P < 0.005$; *cis*, $P < 0.003$, Mann–Whitney *U*-test). There was no significant difference between *trans* [*Sd* +/+ *Skt*^{Gt}] ($n = 23$) and *cis* [*Sd Skt*^{Gt}/+ +] ($n = 10$) mice ($P = 0.956$, Mann–Whitney *U*-test). (B) Histological analyses of vertebral columns in the *Sd* +/+ *Skt*^{Gt} and *Sd Skt*^{Gt}/+ + mutant mice. HE staining of midsagittal sections in thoracic spines of *Sd* +/+ *Skt*^{Gt} (a and c) and *Sd Skt*^{Gt} /+ + (b and d) mice and in sacral spines of *Sd* +/+ *Skt*^{Gt} (e and g) and *Sd Skt*^{Gt}/+ + (f and h) mice. Arrowheads indicate dorsal sides. (c, d, g, and h) Higher magnification of the areas indicated by the boxes in a, b, e, and f, respectively. (C) Whole-mount X-gal staining in the *Sd* +/+ *Skt*^{Gt} and *Sd Skt*^{Gt}/+ + mutant embryos. The β-*gal* expression in the tail notochord of *trans*-heterozygous embryos [*Sd* +/+ *Skt*^{Gt}] at E9.5 (a) and E13.5 (b and c) and of *cis*-heterozygous embryos [*Sd Skt*^{Gt}/+ +] at E9.5 (d) and E13.5 (e and f).

regard to notochord degradation whether *Sd* and *Skt*^{Gt} were in a *trans*- or in a *cis*-configuration.

DISCUSSION

We established a new recessive trap line, B6;CB-*Skt*^{GtAyu8021IMEG}, which had a deformity in caudal IVDs. The insertion site of the trap vector is in the 14th intron of the novel gene *Skt*, located on chromosome 2, near the locus for *Danforth's short tail*. In addition, we found that the enhancer trap locus *Etl4*^{lacZ}, which was previously reported to be an allele of *Sd*, was located in the third intron of the *Skt* gene.

Structure, expression, and function of the *Skt* gene: The sequence of the trapped gene, *Skt*, was obtained using the gene-trap ES clone. The *Skt* gene contains 19 exons encoding a novel protein of 1352 amino acids with a proline-rich region in the N terminus (amino acid positions 298–364) and a coiled-coil domain in the middle (amino acid positions 626–656). Although the role of the proline-rich region in many proteins is not clear yet, a proline-rich region located in the amino-terminal region has been shown to be important for proper folding in cytochrome P450s (mitochondrial, microbial, and microsomal P450s) (KUSANO *et al.* 2001a,b). Thus, the proline-rich region in the Skt protein may have a similar function in protein folding. The coiled-coil motif was first described by CRICK (1952) and by PAULING and COREY (1953) as the main structural element of a large class of fibrous proteins that included keratin, myosin, and fibrinogen, mediating dimerization, heterodimer formation, or trimerization (for a review see LUPAS 1996). These proteins provide a scaffold for regulatory complexes such as tropomyosin and a protective surface for pathogens. As the Skt protein is localized in the cytoplasm, it is conceivable that the Skt protein may provide structural elements or act as a scaffold for regulatory complexes.

Insertion of the gene-trap vector into the 14th intron of the *Skt* gene, downstream of the coiled-coil domain and the proline-rich region, resulted in production of two fusion transcripts with the β-*geo* sequence: one, *Skt-a*,

containing only exons 1–14 and the other, *Skt-b*, lacking 33 bp of the 13th exon from *Skt-a* (see Figure 2B). Northern blot analysis showed that the amount of fusion transcripts from the trapped allele was lower than that of the wild-type allele. Therefore, it is also possible that the insertion of the gene-trap vector resulted in decreased mRNA stability. As tail phenotypes are recessive, insertion of the trap vector may cause a hypomorphic or null mutation, but not a dominant-negative mutation. Although we detected four types of mRNA transcribed from the wild-type *Skt* allele, further analysis will be required to elucidate the function of these mRNA.

The expression patterns of the *Skt* gene can be monitored by X-gal staining, because the expression of the reporter gene, β-*geo*, is under control of the regulatory region of the *Skt* gene. At E11.5, β-*geo* was expressed mainly in the notochord and mesonephros at high levels, and in other tissues as described in the RESULTS. In the $Etl4^{lacZ}$ line, the *lacZ* reporter gene was also expressed in two main tissues, the notochord and the mesonephros (ZACHGO *et al.* 1998). In both lines, *lacZ* expression was first detected at E8.5 in the presumptive notochord cells. In the $Etl4^{lacZ}$ line, *lacZ* expression was detected in the future IVDs at E13.5 and persisted up to E14.5. However, no *lacZ* expression was detected in the IVDs of newborn and adult mice. On the other hand, *lacZ* expression in the IVDs persisted to adult stage in the Skt^{Gt} line. These results suggest that the enhancer located near the $Etl4^{lacZ}$ locus is not sufficient to express the *lacZ* gene in the IVDs of adult mice.

Histochemical analyses of the vertebral column revealed the differences between *Sd* mice and Skt^{Gt} mice. As histological data on $Etl4^{lacZ}$ mice were not described by ZACHGO *et al.* (1998), it is not clear whether the IVD histology is similar to that seen in *Sd* or Skt^{Gt} mice. As reported previously, the development of both the vertebral column and the urogenital system is affected in *Sd* mutation, suggesting that the *Sd* gene is required for formation of derivatives from both the paraxial and the intermediate mesoderm. In addition, both vertebral bodies and IVDs are affected in *Sd* mice. The notochord shows discontinuities as early as E9.5, resulting in the total absence of the nucleus pulposus at all levels and is replaced by peripheral fibers similar to those of the annulus fibrosus in *Sd* adult mice. All vertebral bodies are reduced in a dorso-ventral direction and the number of tail vertebrae is reduced, leading to shortening or absence of the tail. However, in Skt^{Gt} mice, the compression and dislocation of the nucleus pulposus were first observed at E17.5 and were restricted to the tail region. Interestingly, the size of the nucleus pulposus was similar to that in wild-type mice until birth. After birth, the nucleus pulposus did not expand and was dislocated to the periphery, resulting in a kinky-tail phenotype in adults. These observations suggest that *Sd* acts at an early stage of mesoderm development involving both sclerotome and notochord development and that *Skt* acts during the fetal period and at the later stage involving growth and hypertrophy of the nucleus pulposus. Although massive apoptosis in notochord cells was observed in embryos with targeted disruption of *Jun* (BEHRENS *et al.* 2003) or $Sox5^{-/-}/Sox6^{-/-}$ (SMITS and LEFEBVRE 2003), no apoptotic notochord cells were observed in the $Skt^{Gt/Gt}$ embryos at E16.5 and in neonatal mice. Thus, apoptosis is not the cause of compression or dislocation of the nucleus pulposus in Skt^{Gt} mice. As the Skt protein contains the coiled-coil motif that is involved in the formation of mechanically rigid structures, it is possible that the nucleus pulposus lacking Skt protein may not be capable of sustaining mechanical loads, leading to compression or dislocation of the nucleus pulposus.

Although the IVD is formed from two components of developmentally different origins, the nucleus pulposus and the annulus fibrosus, interaction of the nucleus pulposus and annulus fibrosus is not clear yet. In *Sd* mice, disappearance of the notochord cells occurs at early stages of development. THEILER (1988) reported that the fibers of the annulus fibrosus are reduced in *Sd* heterozygous embryos and newborns. However, our results suggest that the annuli fibrosi are not reduced in *Sd* heterozygous adult mice. Thus, the annulus fibrosus may be able to completely compensate for the loss of the nucleus pulposus during growth after birth. In Skt^{Gt} mice, the thin annulus fibrosus was observed together with abnormalities in the nucleus pulposus. At present, it is not known whether the thin annulus fibrosus is caused by the direct effect of *Skt* deficiency or indirectly caused by defects in the nucleus pulposus.

The relationship among the Skt^{Gt}, $Etl4^{lacZ}$, and *Sd* mutations: Our breeding studies revealed that the genetic distance between the *Skt* and *Sd* loci was 0.95 cM. We believe that the *Skt* gene is distinct from the *Sd* gene for the following reasons. First, anti-Skt antibody detected the predicted size of protein deduced from the *Skt* gene. If the *Skt* was part of the *Sd* gene, we should have detected a larger protein by Western blot analysis. But, we could not detect any such protein. Second, our *trans–cis* test demonstrated that both double heterozygotes exhibited indistinguishable phenotypes, regardless of whether *Sd* and Skt^{Gt} were in a *trans*- or a *cis*-configuration. On the basis of the results by ZACHGO *et al.* (1998), *Sd* is a gain-of-function mutation. As the *Skt* is a recessive mutation, producing a hypomorphic or null allele, the *Sd* phenotype is expected to be attenuated in the *cis*-configuration. Therefore, the phenotype in double heterozygotes in the *trans*-configuration might be more severe than that in the *cis*-configuration if the *Skt* gene is part of the *Sd* gene.

We have shown that the $Etl4^{lacZ}$ locus is located in the third intron of the *Skt* gene. Interestingly, a sequence that has 93% homology to consensus sequence 3 (CS3) in node/notochord enhancers of *Hnf3*β (NISHIZAKI *et al.* 2001) was found in the fourth intron of the *Skt* gene, located 106 kb downstream of the insertion site of

Etl4^{lacZ}. As the expression patterns of *Etl4*^{lacZ} are quite similar to those in *Skt*^{Gt} mice and as *Etl4*^{lacZ} mice have similar kinks in the tail region (Zachgo *et al.* 1998), the *lacZ* gene in the enhancer trap vector may be expressed under the control of this possible node/notochord enhancer. Zachgo *et al.* (1998) reported that the *Etl4*^{lacZ} locus is localized ~0.75 cM distal to *Sd* and that the *Sd* phenotype is attenuated when *Etl4*^{lacZ} is present in *cis*. These results suggest that the possible enhancer sequence in the fourth intron of the *Skt* gene functions also as the enhancer for the *Sd* gene and that the insertion of an enhancer trap vector in the third intron, as found in the *Etl4*^{lacZ} line, may eliminate the enhancer function for the *Sd* gene, resulting in the attenuation of the *Sd* phenotype.

Future study on the functions of the Skt and Sd proteins may provide important clues for understanding the mechanisms for the development of notochordal cells and their differentiation into the nucleus pulposus cells.

We thank T. Iwamura, K. Miike, K. Haruna, and H. Hino for helpful and critical discussions and comments on the manuscript, and Michiyo Nakata and Ikuyo Kawasaki for technical assistance. This work was supported in part by a Grant-in-Aid on Priority Areas from the Ministry of Education, Science, Culture, and Sports of Japan and a grant from the Osaka Foundation for Promotion of Clinical Immunology.

LITERATURE CITED

Alfred, J. B., K. Rance, B. A. Taylor, S. J. Phillips, C. M. Abbott *et al.*, 1997 Mapping in the region of Danforth's short tail and the localization of tail length modifiers. Genome Res. **7:** 108–117.

Allen, N. D., D. G. Cran, S. C. Barton, S. Hettel, W. Reik *et al.*, 1988 Transgenes as probes for active chromosomal domains in mouse development. Nature **333:** 852–855.

Ang, S., and J. Rossant, 1994 HNF-3β is essential for node and notochord formation in mouse development. Cell **78:** 561–574.

Araki, K., T. Imaizumi, T. Sekimoto, K. Yoshinobu, J. Yoshimuta *et al.*, 1999 Exchangeable gene trap using the Cre/mutated lox system. Cell. Mol. Biol. **45:** 737–750.

Aszodi, A., D. Chan, E. Hunziker, J. F. Bateman and R. Fassler, 1998 Collagen II is essential for the removal of the notochord and the formation of intervertebral discs. J. Cell Biol. **143:** 1399–1412.

Behrens, A., J. Haigh, F. Mechta-Grigoriou, A. Nagy, M. Yaniv *et al.*, 2003 Impaired intervertebral disc formation in the absence of *Jun*. Development **130:** 103–109.

Chiang, C., Y. Litingtung, E. Lee, K. E. Young, J. Corden *et al.*, 1996 Cyclopia and defective axial patterning in mice lacking Sonic hedgehog gene function. Nature **383:** 407–413.

Crick, F. H., 1952 Is alpha-keratin a coiled coil? Nature **170:** 882–883.

Dunn, L. C., S. Gluecksohn-Schoenheimerl and V. Bryson, 1940 A new mutation in the mouse affecting spinal column and urogenital system. J. Hered. **31:** 343–348.

Gerard, R. D., and Y. Gluzman, 1985 New host cell system for regulated simian virus 40 DNA replication. Mol. Cell. Biol. **5:** 3231–3240.

Gossler, A., A. L. Joyner, J. Rossant and W. C. Skarnes, 1989 Mouse embryonic stem cells and reporter constructs to detect developmentally regulated genes. Science **244:** 463–465.

Gruneberg, H., 1953 Genetical studies on the skeleton of the mouse. VI. Danforth's short-tail. J. Genet. **51:** 317–326.

Gruneberg, H., 1958 Genetical studies on the skeleton of the mouse. XXII. The development of Danforth's short-tail. J. Embryol. Exp. Morphol. **6:** 124–148.

Hogan, B., R. Beddington, F. Costantini and E. Lacy, 1994 *Manipulating the Mouse Embryo: A Laboratory Manual*, pp. 379–381. Cold Spring Harbor Laboratory Press, Cold Spring Harbor, NY.

Korn, R., M. Schoor, H. Neuhaus, U. Henseling, R. Soninenen *et al.*, 1992 Enhancer trap integrations in mouse embryonic stem cells give rise to staining patterns in chimaeric embryos with a high frequency and detect endogenous genes. Mech. Dev. **39:** 95–109.

Kozak, M., 1996 Interpreting cDNA sequences: some insights from studies on translation. Mamm. Genome **7:** 563–574.

Kusano, K, N. Kagawa, M. Sakaguchi, T. Omura and M. R. Waterman, 2001a Importance of a proline-rich sequence in the amino-terminal region for correct folding of mitochondrial and soluble microbial p450s. J. Biochem. **129:** 271–277.

Kusano, K., M. Sakaguchi, N. Kagawa, M. R. Waterman and T. Omura, 2001b Microsomal p450s use specific proline-rich sequences for efficient folding, but not for maintenance of the folded structure. J. Biochem. **129:** 259–269.

Lane, P. W., and C. S. Birkenmeiser, 1993 Urogenital syndrome (*us*): a developmental mutation on chromosome 2 of the mouse. Mamm. Genome **4:** 481–484.

Langman, J., 1969 *Medical Embryology*, pp. 134–135. Williams & Wilkins, Baltimore.

Lupas, A., 1996 Coiled coils: new structures and new functions. Trends Biochem. Sci. **21:** 375–382.

Lupas, A., M. Van Dyke and J. Stock, 1991 Predicting coiled coils from protein sequences. Science **252:** 1162–1164.

Maatman, R., J. Zachgo and A. Gossler, 1997 The Danforth's short tail mutation acts cell autonomously in notochord cells and ventral hindgut endoderm. Development **124:** 4019–4028.

Nishizaki, Y., K. Shimazu, H. Kondof and H. Sasaki, 2001 Identification of sequence motifs on the node/notochord enhancer of Foxa2 (Hnf3β) gene that are conserved across vertebrate species. Mech. Dev. **102:** 57–66.

Niwa, H., K. Yamamura and J. Miyazaki, 1991 Efficient selection for high-expression transfectants with a novel eukaryotic vector. Gene **108:** 193–200.

Paavola, L. G., D. B. Wilson and E. M. Center, 1980 Histochemistry of the developing notochord, perichordal sheath and vertebrae in Danforth's short-tail (*Sd*) and normal C57BL/6 mice. J. Emboryol. Exp. Morphol. **55:** 227–245.

Pauling, L., and R. B. Corey, 1953 Compound helical configurations of polypeptide chains: structure of proteins of the alpha-keratin type. Nature **171:** 59–61.

Rufai, A., M. Benjamin and J. R. Ralphs, 1995 The development of fibrocartilage in the rat intervertebral disc. Anat. Embryol. **192:** 53–62.

Smits, P., and V. Lefebvre, 2003 Sox5 and Sox6 are required for notochord extracellular matrix sheath formation, notochord cell survival and development of the nucleus pulposus of intervertebral discs. Development **130:** 1135–1148.

Theiler, K., 1988 Vertebral malformations. Adv. Anat. Embryol. Cell Biol. **112:** 1–99.

Wilson, V., L. Manson, W. C. Skarnes and R. S. Beddington, 1995 The T gene is necessary for normal mesodermal morphogenetic cell movements during gastrulation. Development **121:** 877–886.

Zachgo, J., R. Korn and A. Gossler, 1998 Genetic interactions suggested that Danforth's short tail (Sd) is a gain-of-function mutation. Dev. Genet. **23:** 86–96.

Communicating editor: C. A. Kozak